36th AIAA Fluid Dynamics Conference and Exhibit
5 - 8 June 2006, San Francisco, California

AIAA 2006-3914

36th AIAA Fluid Dynamics Conference and Exhibit, San Francisco, CA, Jun. 5–8, 2006

Subsonic Flow over Unstalled Pitching Airfoil Computed by Euler Method

Shuchi Yang*, Shijun Luo†, Feng Liu‡
Department of Mechanical and Aerospace Engineering
University of California, Irvine, CA 92697-3975
Her-Mann Tsai§
Temasek Laboratories
National University of Singapore
Kent Ridge Crescent, Singapore 119260

Subsonic flow about a sinusoidally pitching airfoil with mean angle of attack is studied by an unsteady compressible Euler flow solver. Fully attached flows are considered. The Euler method is evaluated extensively by wind-tunnel test data of two no-stall cases for pitching-oscillating airfoil NACA 0012 in the literature. The wind tunnel walls are not considered in the computations. The boundary layer effects are identified. The effects of mean angle of attack on the fluctuating forces are studied.

I. Introduction

In many engineering applications, e.g., helicopter rotors, turbomachinery, and wind turbines, airfoils experience dynamic pitching motion. McCroskey et al.[1] observed experimentally that compressibility can play a role in pitching airfoil performance: when the angle of attack of an airfoil increases, the acceleration of the flow that occurs around the leading edge can result in flow velocities four to five times greater than the free-stream value. Thus, a freestream flow of Mach number as low as 0.18 can induce sonic velocity on an airfoil pitching dynamically to high angles of attack.

McAlister, Pucci, McCroskey, and Carr[2] performed an extensive experimental investigation of eight airfoil profiles including more than 50 combinations of subsonic free-stream Mach numbers and parameters of the sinusoidal pitching oscillation. The surface pressure distribution, as well as the lift, drag, and pitching moment derived therefrom, are displayed both in and out of stall. Fung and Carr[3] studied the observed behavior of the flow around a pitching-oscillating NACA 0012 airfoil with an amplitude of 10° and mean angle of attack of 15° before separation. They found that the parametric dependency of separation on frequency for supercritical flows is different from that for subcritical flows. For subcritical flows, increasing the reduced frequency delays separation of the boundary layer and, hence, allows the airfoil to attain high minimum pressure coefficient at higher angles of attack. However, for supercritical flows, the formation of a local supersonic region and the associated shock can occur at a location close to the leading edge. The vortical content of the flow is intensified due to the relatively short extension of the local supersonic region. The local outer flow and the boundary layer are no longer stable. Hence, compressibility effects pose a limit on pressure suction enhancement by increasing unsteadiness.

Many important features of unsteady airfoil behavior can be described by linearized thin-airfoil theory. Garrick[4] used Theodorsen's incompressible small oscillatory flat-plate theory[5] and developed compact expressions for forces, moments, and input power. Closed forms for the corresponding load distributions were derived by Biot,[6] and presented in the book of Fung.[7] Oscillating airfoils at subcritical speeds, that is, when

*Post-Doctoral Researcher. AIAA senior member
†Researcher.
‡Professor. Associate Fellow AIAA.
§Principal Research Scientist, AIAA Member

the flow remains subsonic everywhere, are not fundamentally different from their incompressible counterparts, but no analytical expressions are obtained. McCroskey[8] showed a representative example supplied by S.R. Bland. Kutta condition is enforced at the trailing edge in the linearized oscillating-airfoil theory.

A hierarchy of computational approaches has been developed for studying compressible flows about flapping airfoils. It ranges from Euler method,[9,10] and Navier-Stokes code.[11,12] Young and Lai[13] found that compressibility effect occurs at high frequencies using a compressible Navier-Stokes computations. They showed that the free-stream Mach number used in the simulations has an important effect on the forces predicted for both pitching and plunging oscillations, although no significant influence on the wake structures was observed in the simulations.

The wake of a flapping airfoil actually consists of a viscous part and an inviscid part.[14] The viscous wake is the result of merging of two boundary layers on the airfoil. The viscous wake is limited in a very thin region at Reynolds numbers of $10^4 \sim 10^5$. The inviscid wake is due to the presence of the airfoil in the flow with a changing angle of attack and represents a propulsive vortical signature of the flapping airfoil.

It is known that the Euler method can capture automatically the shear layer separated from the sharp trailing edge and its spirally rolling up into wake vortices. No Kutta condition is needed to apply in the Euler method. Very recently, the authors used an Euler solver to compute[15] the time-averaged thrust coefficient of a plunging NACA 0012 airfoil for various plunging amplitudes at free-stream Mach number of 0.3 and reduced frequency ranging from 0.125 to 1.5. The computed thrusts with a subtraction of the quasi-steady skin friction of flat plate agree well with the Navier-Stokes computational results obtained by Tuncer et al.,[11] provided that there occurs no boundary-layer separation over the airfoil.

To the authors' knowledge, although subsonic flows about pitching airfoil have been studied by numerous computational codes, no systematic evaluations with existing standard test data base have been published. The objective of the present investigation is to evaluate the unsteady compressible Euler method for simulating the no-stall cases of the data base of Ref. 2 suggested by McCroskey and Pucci.[16] In the following sections, the Euler method is first presented and then applied for the evaluations. Lastly conclusions are drawn.

II. Euler Method

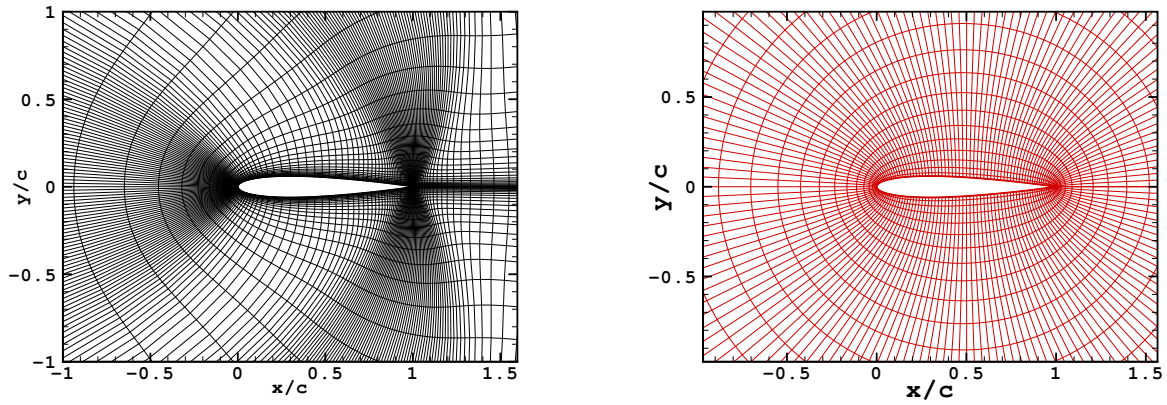

(a) 577 × 65 C-grid

(b) 321 × 65 O-grid

Figure 1. Close-up view of the for pitching NACA 0012 airfoil, only every other line is plotted.

It is known that the Euler method can capture automatically the inviscid wake produced by the unsteady motion of a sharp trailing-edge airfoil. Although the boundary layer together with the viscous wake are absent in the Euler solutions, the primary trailing-edge vortex configurations and their interactions with the moving body surface are reproduced as long as there are no significant boundary-layer separations.

The present Euler solver is based on a multi-block, multigrid, finite-volume method and parallel code for the three-dimensional, compressible steady and unsteady Euler and Navier-Stokes equations. The method

uses central difference with a blend of second- and fourth-order artificial dissipation and explicit Runge-Kutta-type time marching. The coefficients of the artificial dissipation depend on the local pressure gradient. The order of magnitude of the added artificial dissipation terms is of the order of the truncation error of the basic scheme, so that the added terms have little effect on the solution in smooth parts of the flow. Near the steep gradients the artificial dissipation is activated to mimic the physical dissipation effects. Unsteady time-accurate computations are achieved by using a second-order accurate implicit scheme with dual-time stepping. The solution for each real-time step is solved by an explicit time-marching scheme in a fictitious time in which the local time stepping, residual smoothing, and multigrid techniques can be used to accelerate convergence to a steady state. The resulting code preserves symmetry.[17]

On the airfoil surface the instantaneous flow normal velocity component is set equal to the local surface normal velocity component prescribed by the oscillatory motion. The far field boundary is located at $20c$ away from the airfoil. At the far-field inflow and outflow boundaries the flow variables are evaluated using the first-order Riemann invariant extrapolation. The initial condition is the airfoil starting from a position in its oscillatory motion in a free-stream flow and unique solution is obtained for any position used for the initial condition. The solver has been validated for a number of steady and unsteady cases.[10,18–22]

Two grids are used in the computations of a pitching NACA 0012 airfoil. One grid is a C-type grid, 577×65. There are 385 grid points around the airfoil, and 97 grid points in the wake. The other grid is of O-type, 321×65. Close-up views of the C-grid and O-grid are shown in Fig. 1. Only every other line is plotted in the figures for clarity. The C-type grid yields aerodynamic forces which are grid-independent as shown by the numerical experiments in Reference 10. The O-grid yields almost the same aerodynamic forces as the C-grid, but needs much less computer time. Numerical experiments of time-step refinement were also performed and the solutions with 64 steps per cycle are time-step independent. For freestream Mach numbers between 0.05 and 0.3, about five cycles of computations are needed for the transients to disappear.

It is known that flow bifurcation appears in pure plunge at zero mean angle of attack when the maximum instantaneous angle of attack is extremely large. Jones et al.[23] reported a deflected vortex street and a non-zero time-averaged lift for the case $k = 6.15, h = 0.12$, i.e., having a maximum effective angle of attack equal to 55.9°, in water-tunnel experiments and reproduced this phenomena by a potential-flow code using different initial conditions. Lewin et al.[24] also demonstrated the flow switching by a viscous-flow code. For the cases without dynamic stall, the numerical solutions of the Euler solver are independent of the initial conditions.

III. Computational Models

Consider an airfoil of chord c performing a sinusoidal pitching oscillation about the quarter-chord point from the leading edge in a uniform free stream of velocity U_∞ and Mach number M_∞. The instantaneous angle of attack is α, which is positive in the nose-up direction.

$$\alpha(t) = \alpha_0 + \alpha_1 \sin(\omega t). \tag{1}$$

where t is physical time, α_0 is the mean angle of attack, α_1 and ω are the amplitude and the angular frequency of the pitching oscillation, respectively. Maximum angle of attack, $\alpha_{max} = \alpha_0 + \alpha_1$. Pitch-up and pitch-down mean the increase and decrease of the instantaneous angle of attack, respectively. The reduced frequency is defined as $k = \omega c/2U_\infty$.

The instantaneous pressure coefficient is c_p. The instantaneous loading coefficient is $\Delta c_p = (c_p)_{lower} - (c_p)_{upper}$. The instantaneous lift coefficient is c_l. The instantaneous pitching moment coefficient about the quarter-chord point is c_m (positive when clockwise). The instantaneous pressure thrust coefficient is c_t. The instantaneous input power coefficient is $c_{ip} = -c\dot{\alpha}c_m/U_\infty$, where a dot denotes a differentiation with respect to t.

IV. Evaluation of Euler Method by Experimental Data Base

The Euler method is evaluated by the experimental data base[2] in this section. Two test cases from the no-stall region are computed by the Euler method. They are proposed by McCroskey et al.[16] as standard data base for evaluating computational methods and theoretical models.

Case 1: NACA 0012, $\alpha_0 = 4.93°$, $\alpha_1 = 4.99°$, $k = 0.198$, $M_\infty = 0.301$, $Re = 3.91 \times 10^6$.

Case 2: NACA 0012, $\alpha_0 = 7.978°$, $\alpha_1 = 4.91°$, $k = 0.199$, $M_\infty = 0.301$, $Re = 3.89 \times 10^6$.

The maximum angle of attack is $\alpha_{max} \approx 10^\circ$ and 13° in Case 1 and 2, respectively. The dynamic stall onset is at $\alpha_{max} = 14^\circ$ as shown in Ref. 16 and, thus, no dynamic stall occurs in either case.

The static-stall angle of attack for the NACA 0012 airfoil under the same conditions is 13.7°.[1] For the pure pitching oscillation, the dynamic-stall angle of attack is nearly equal to the static-stall angle of attack. Unlike pure plunging, the pitching motion of the airfoil does not raise the stall angle of attack. Due to the rotational velocity of the airfoil $\dot{\alpha}$, a distribution of varying angle of attack along the airfoil chord is formed in addition to the uniform angle of attack. When the airfoil starts to rotate counter-clockwise from its maximum angle of attack, $\dot{\alpha} < 0$, which produces an increment to the local angle of attack at the airfoil leading edge and tends to activate a dynamic stall. In the mean time the rotational acceleration $\ddot{\alpha} < 0$, which produces a pure couple in the clockwise direction (See Section 13.4 of Fung[7]) and furthers the tendency towards dynamic stall.

The tests[2] were performed in a solid-wall wind tunnel. The surface pressure were measured, and the lift, drag, and pitching moment were derived therefrom. The free-stream Mach number was approximately 0.30 and the Reynolds number was 4×10^6 based on chord. The effects of the tunnel walls were estimated to be small, but not negligible. They were not corrected in the test report in view of the uncertainty of applying standard wall correction to cases with large angles of attack and with possible separation.

The Euler computations are made with free air conditions. The wind-tunnel wall is not considered in the computations. The unsteady pressure and load distributions are studied first. Then the unsteady forces and moment are investigated. At last, the effects of the mean angle of attack are discussed. The inviscid thrusts (or drag) computed from the Euler method can be compared directly with the test data, since the data were obtained through integrating the surface pressures. The Euler numerical results are also compared with those of the incompressible linearized theory if available.

A. Pressure Distributions

The computed instantaneous pressure coefficients c_p on upper and lower surfaces of the pitching airfoil NACA 0012 versus x/c and ωt or α or for Case 1 and Case 2 are presented in Fig. 2, where the increment of ωt is 11.25°. When ωt increases from -90° to 90° the airfoil is pitching up. When ωt increases from 90° to 270° the airfoil is pitching down. The critical pressure coefficient of the free-stream flow calculated using the isentropic flow formula is marked as c_p^* in Fig. 2. This indicates that Case 1 is subcritical and Case 2 is supercritical. A local supersonic region appears over upper surface near the leading edge when $56.25^\circ \leq \omega t \leq 157.5^\circ$ in the computational results of Case 2. The measured supersonic region[2] occurs when $46^\circ \leq \omega t \leq 150^\circ$ in Case 2. They are reasonably close to each other. The local supersonic region spans about one third of the entire cycle.

Table 1 Comparison of the computed minimum pressure coefficients $(c_p)_{min}$, maximum Mach number M_{max} and the angle of attack α at which they occur.

	Computations			Experiments[2]		
Case	$(c_p)_{min}$	M_{max}	α	$(c_p)_{min}$	M_{max}	α
1	-5.02	0.83	9.90°	-6.1	0.922	9.9°
2	-9.12	1.25	12.9°	-9.1	1.232	12.9°

The computed and measured minimum pressure coefficient, $(c_p)_{min}$, maximum Mach number M_{max} and the angle of attack, α at which they occur over a cycle of the pitching airfoil NACA 0012 are compared in Table 1. The agreements are excellent for Case 2, but not so for Case 1. The reason for the discrepancy in Case 1 is attributed to the leading-edge boundary-layer effects. According to Ref. 16, in Case 1, the boundary layers on both the upper and lower surfaces were fully attached throughout the cycle, except for a small separation bubble near the upper surface leading edge for $\alpha \geq 5^\circ$, which produced transition from laminar to turbulent flow. For Case 2, no such a leading-edge boundary-layer effect was observed.[16]

The computed pressure distribution with maximum suction, i.e., at the instant when $(c_p)_{min}$ occurs is plotted and compared with the measured upper-surface pressure distribution. Fig. 3 presents the computed instantaneous pressure coefficient c_p on the upper and lower surfaces of the pitching NACA 0012 airfoil versus x/c and $(x/c)^{1/2}$ for Case 1 and Case 2 at the instant when $(c_p)_{min}$ occurs compared with the experimental data,[2] where $(x/c)^{1/2}$ is used to stretch out the leading-edge region where the variations are the greatest. The measured lower-surface pressure distributions are not available to the present authors. As shown by

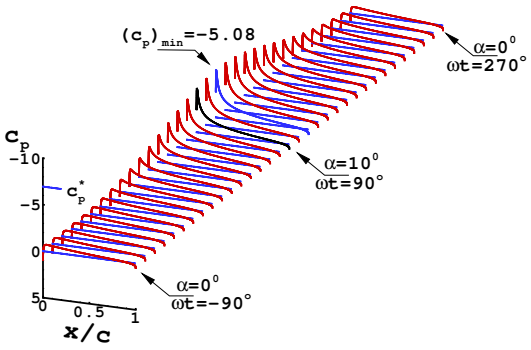

(a) Upper surface for Case 1

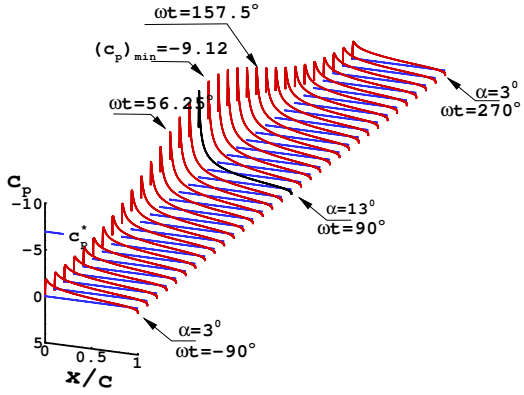

(b) Upper surface for Case 2

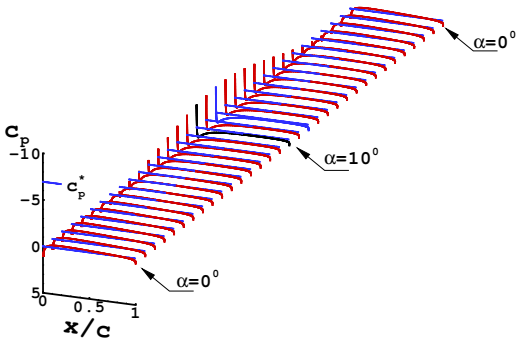

(c) Lower surface for Case 1

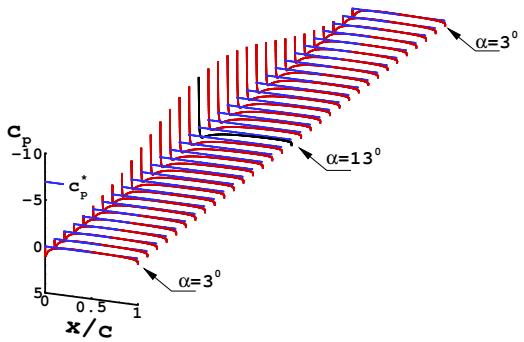

(d) Lower surface for Case 2

Figure 2. Computed pressure coefficient c_p on the surface in a pitching cycle.

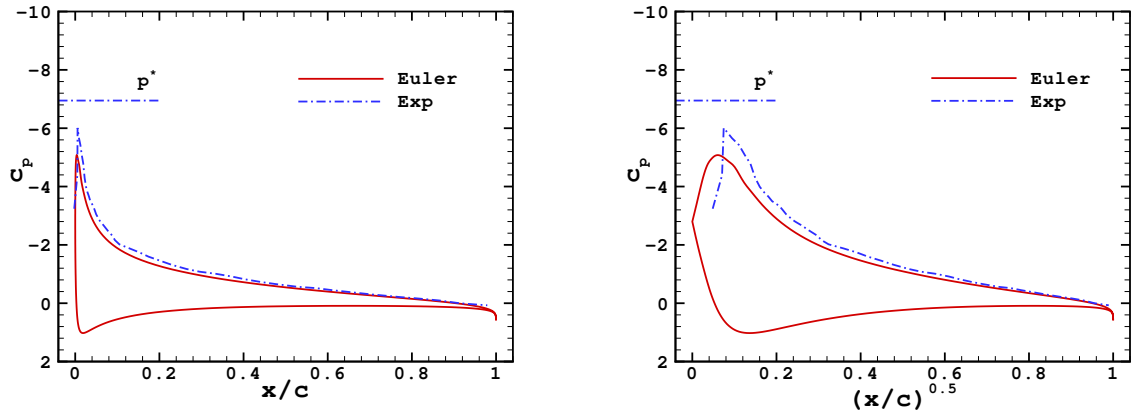

(a) Case 1

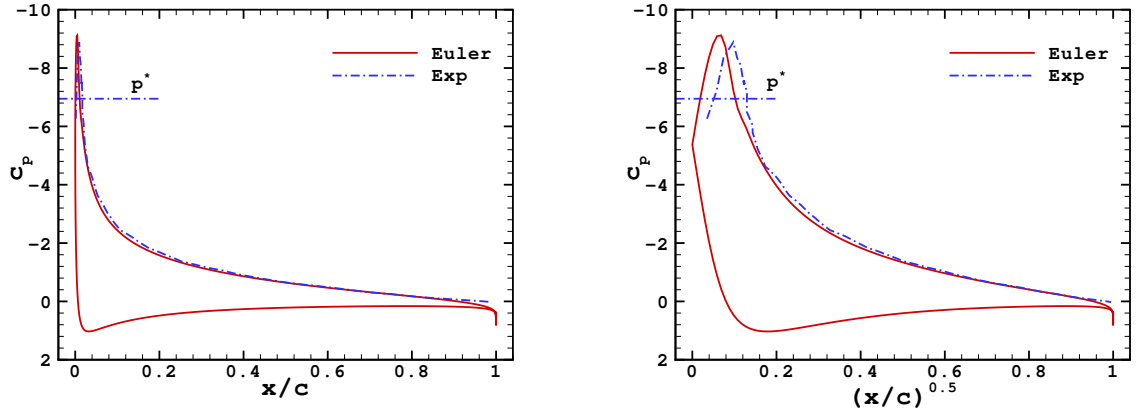

(b) Case 2

Figure 3. Computed pressure coefficient c_p at the instant of $(c_p)_{min}$ compared with experiments.[2]

the figures, the measured minimum pressure coefficient locations shift in the down-streamwise direction by a small distance of the order 0.03% of the airfoil chord for both Case 1 and Case 2. This shift may be due to the wind-tunnel wall effect. The discrepancy in the magnitude of $(c_p)_{min}$ for Case 1 is attributed to the effects of the boundary layer effect as discussed above.

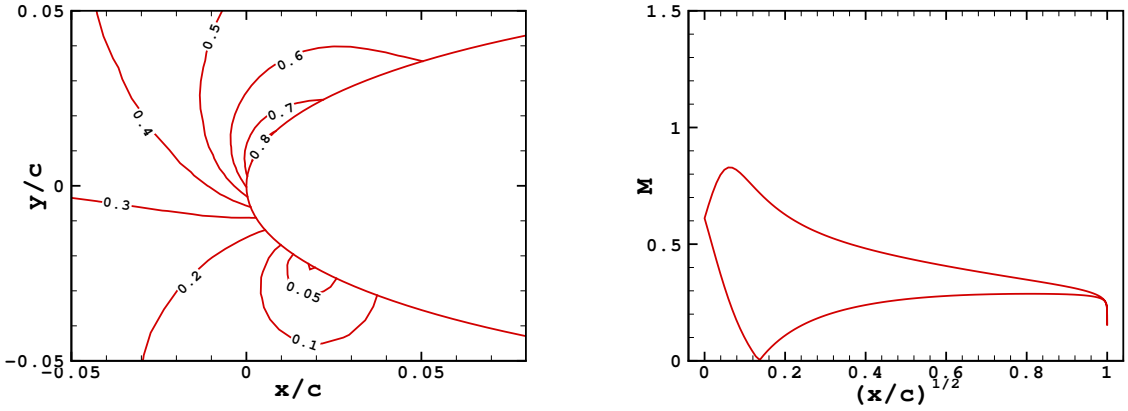

(a) Case 1

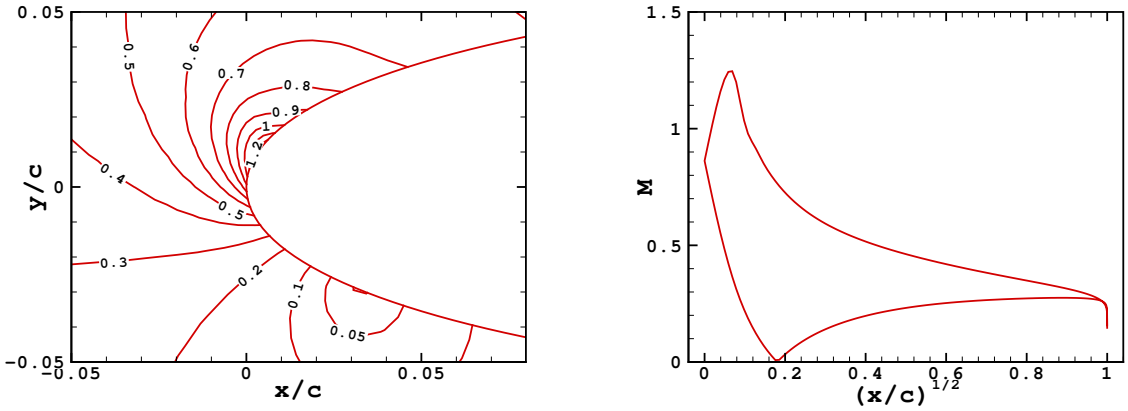

(b) Case 2

Figure 4. Computed Mach number contours and surface Mach number distributions at the instant when $(c_p)_{min}$ occurs .

The computed Mach number contours in the neighborhood of the leading edge and the surface Mach number distribution at the instant when $(c_p)_{min}$ occurs are shown in Fig. 4. The maximum Mach number on the upper surface is 0.83 and 1.25 for Case 1 and Case 2, respectively.

The top figures of Fig. 4 show in detail the developing compressible flow field around the leading edge of the pitching NACA 0012 airfoil. The stagnation point on the lower surface is easily discernible at the center of the smallest closed contour of $M = 0.01$. The flow accelerates as it progresses around the leading edge, as represented by the closely spaced contours emanating from the leading edge region. As the flow continues to move around the airfoil, it continues to accelerate, until the surface curvature decreases, where a plateau appears in the the Mach-number contours. This region shows very little gradient along the airfoil surface. In Case 2, the $M = 1.0$ contour with the enclosed upper surface forms a local supersonic region. No shock wave is found in Fig. 4, which agrees with the shadowgragh observation of Refs. 2 and 3.

The pressure distribution with maximum suction occurs near maximum angle of attack, or $\omega t = 90°$. To further the verification on pressure distribution, three more stations of ωt are considered. In Case 1, $\omega t = 0°$ and 180° correspond to $\alpha = 5°$ in pitch-up and 5° in pitch-down, respectively, and $\omega t = -90°$ corresponds to $\alpha = 0°$ at the end of pitch-down or the beginning of pitch-up. In Case 2, $\omega t = 0°$ and 180° correspond to $\alpha = 8°$ in pitch-up and 8° in pitch-down, respectively, and $\omega t = -90°$ corresponds to $\alpha = 3°$ at the end of pitch-down or the beginning of pitch-up.

Figure 5 presents the pressure coefficient c_p over the upper and lower surfaces of the airfoil at $\omega t = -90°$, 0° and 180° compared with the experimental data[2] on the upper surface. The lower-surface data are unavailable to the present authors.

In Case 1, a distinct discrepancy between the computation and experiment is noted when $\omega t = 180°$, or $\alpha = 5°$ during pitch-down. The peak of c_p near the leading edge on the upper surface is significantly higher in the experimental data. Similar behavior is seen in Fig. 3 for Case 1 and it is attributed to the occurrence of a small laminar-boundary-layer separation bubble over the upper surface near the leading edge when $\alpha \geq 5°$ observed in the test. In Case 2, a distinct discrepancy between the computation and experiment is noted when $\omega t = 180°$ and $\omega t = -90°$ in pitch-down. The peak of c_p near the leading edge on upper surface is significantly lower in the experimental data. This is attributed to the upper-surface boundary layer thickening, especially near the trailing edge due to the increasing α_{max} to 13° observed by McCroskey and Pucci.[16] Otherwise, the agreement between the Euler computations and the experimental data are fair.

B. Harmonic Components of Pressure Distributions

The details of the measured instantaneous pressure distributions were studied by harmonic analysis by McCroskey and Pucci.[16] Accordingly, The computed pressure coefficient, c_p is decomposed into the harmonic components with respect to the motion of the airfoil defined by Eq. (1).

$$c_p = c_{p0} + c_{p1s} sin(\omega t) + c_{p1c} cos(\omega t) + c_{p2} sin(2\omega t + \phi_2) + ... \tag{2}$$

where c_{p0} is the mean value of c_p, c_{p1s} and c_{p1c} are the real and imaginary parts of the first harmonic component, c_{p2} and ϕ_2 are the magnitude and phase of the second harmonic component.

Figure. 6 and 7 present the computed harmonic components of the pressure coefficients on the airfoil surface compared with the experimental data[16] and incompressible linear theory for Case 1 and Case 2, respectively. The Euler computations agree reasonably well with the experimental data. Their discrepancy is mainly associated with those in the magnitude of $(c_p)_{min}$ in Case 1 and the location of $(c_p)_{min}$ in both cases discussed in Subsection A. c_{p2} is small, but not negligible. The first harmonic components dominate and thus, ϕ_2 is not shown and a comparison with the linear theory is justified. In the linear theory, the mean value c_{p0} is comprised of small-disturbance components due to thickness and mean angle of attack, the first harmonic component (c_{p1s}, c_{p1c}) on the upper and lower surface are equal and opposite and all higher harmonic components are zero. The linear theory gives the right qualitative behavior, but is clearly not accurate for the present mean angles of attack, amplitude, airfoil geometry, and M_∞.

Case 1 and Case 2 have nearly the same α_1, k, M_∞ and Re, but different α_0. The mean angle of attack α_0 of Case 2 is greater than that of Case 1. From Fig. 6 and Fig. 7, the fluctuating pressure load of Case 2 is greater than that of Case 1, though the pitching amplitudes α_1 of the two cases are equal. The greater fluctuating pressure load of Case 2 is caused by the larger mean angle of attack. This effect is not seen in the linear theory.

C. Harmonic Components of Fluctuating load Distribution

The details of the fluctuating load distribution are also studied by a harmonic analysis of the instantaneous load distribution, Δc_p along the airfoil chord.

$$\Delta c_p = \Delta c_{p0} + \Delta c_{p1} sin(\omega t + \phi_{p1}) + \Delta c_{p2} sin(2\omega t + \phi_{p2}) + ... \tag{3}$$

where Δc_{p0} is the mean value of Δc_p, Δc_{pi} and ϕ_{pi} are the magnitude and phase of the i-th harmonic component of Δc_p.

The mean load, Δc_{p0} is not shown. Fig. 8 presents the computed harmonic components of fluctuating load distribution compared with the experimental data and incompressible linear theory. The experimental

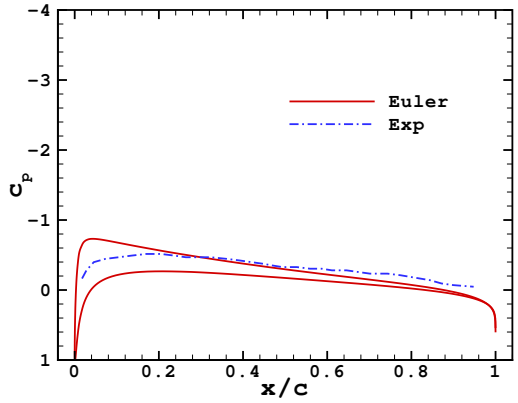

(a) Case 1 ($\omega t = -90°$)

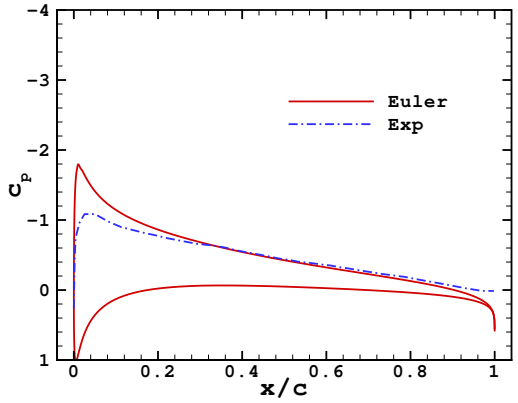

(b) Case 2 ($\omega t = -90°$)

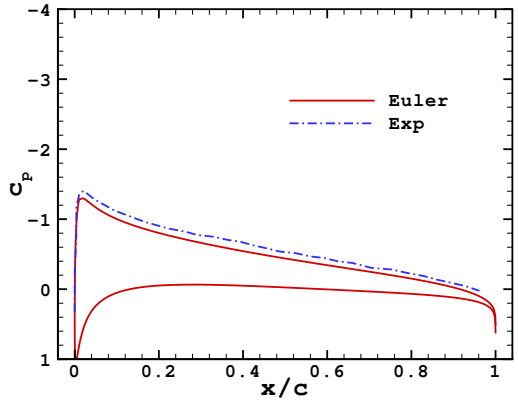

(c) Case 1 ($\omega t = 0°$)

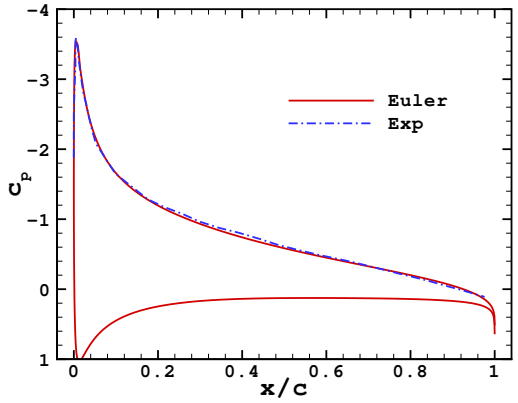

(d) Case 2 ($\omega t = 0°$)

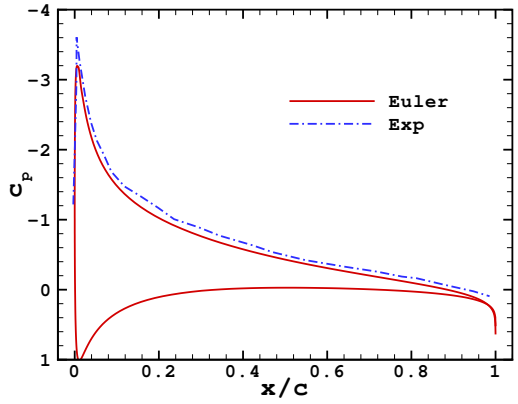

(e) Case 1 ($\omega t = 180°$)

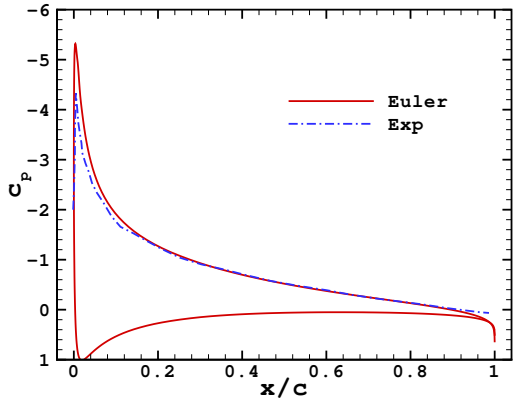

(f) Case 2 ($\omega t = 180°$)

Figure 5. Computed instantaneous pressure coefficient c_p at $\omega t = -90°$, $0°$ and $180°$ compared with experimental data.[2]

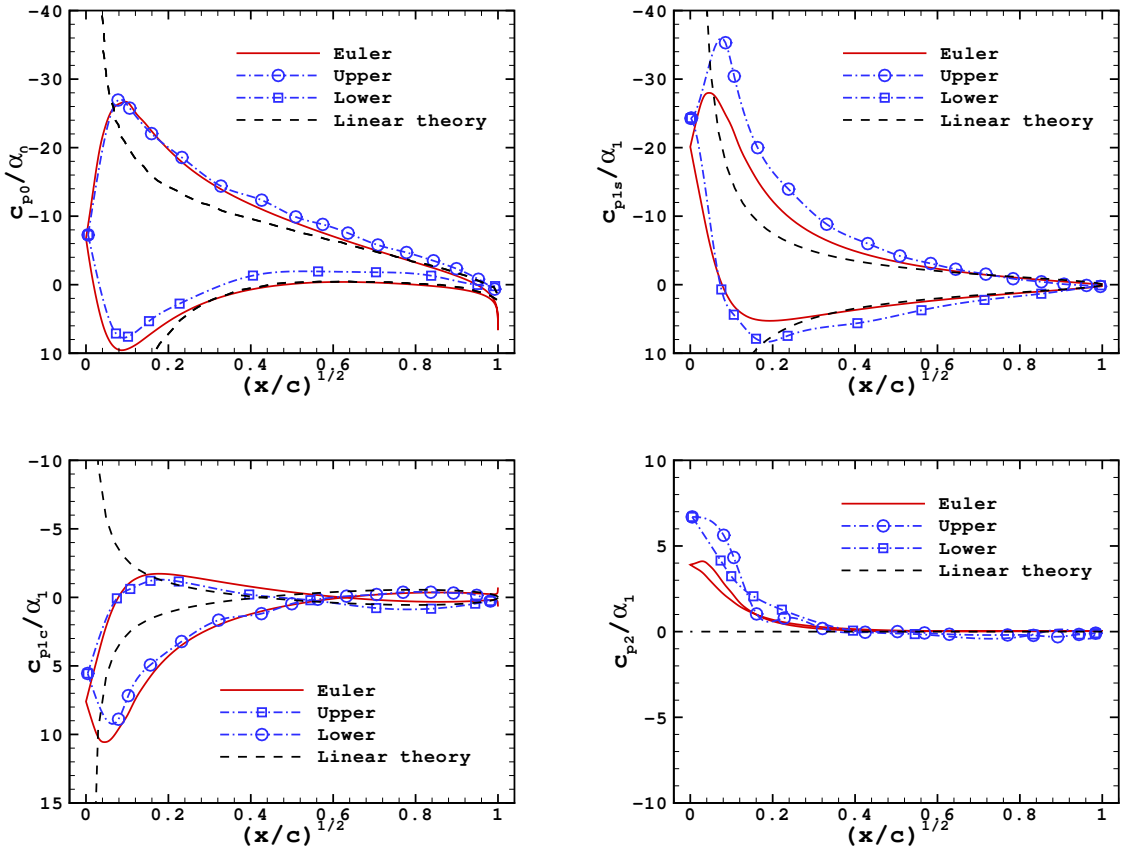

Figure 6. Comparison of harmonic components of pressure distributions on airfoil surface for Case 1.

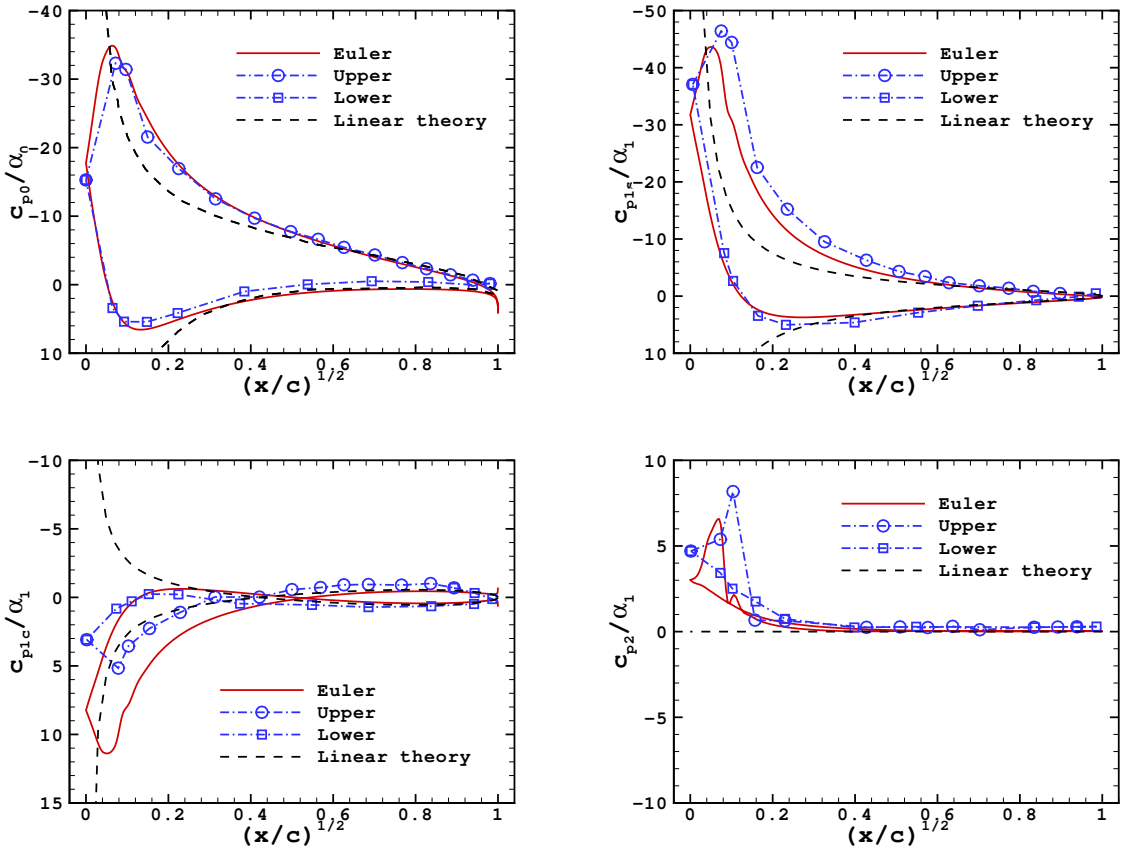

Figure 7. Comparison of harmonic components of pressure distributions on airfoil surface for Case 2.

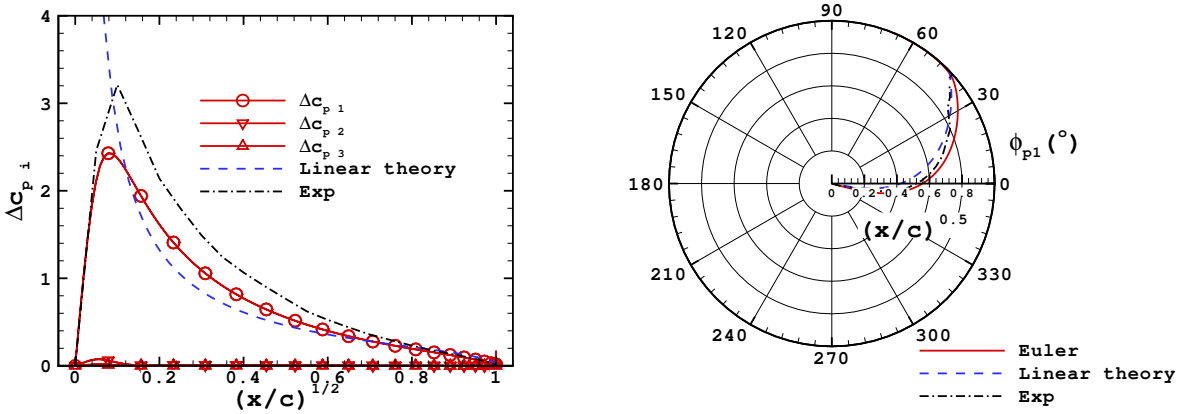

(a) Case 1

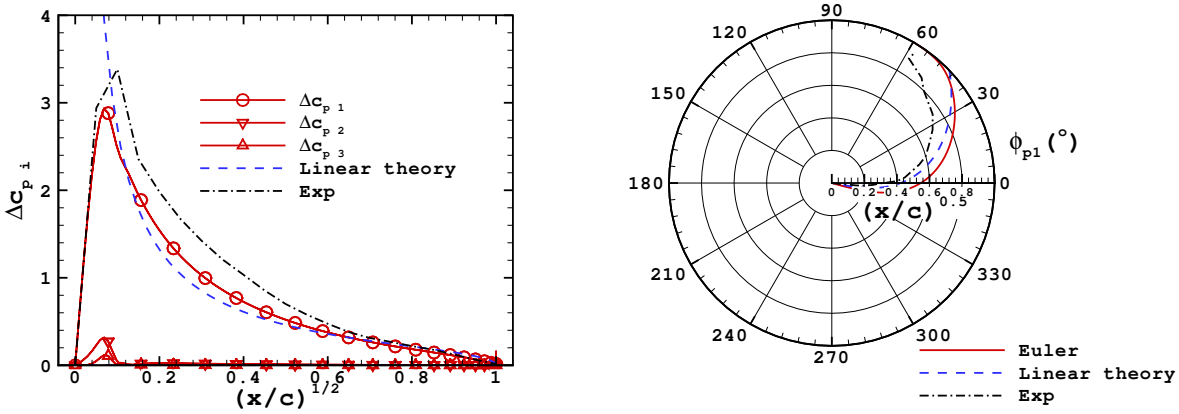

(b) Case 2

Figure 8. Harmonic components of fluctuating load distribution.

data of Δc_{p1} and ϕ_{p1} were not given in Ref. 2. They are calculated from the given test data of c_{p1s} and c_{p1c} over the upper and lower surfaces. In both the Euler solutions and the experimental results, the first harmonic component dominates and thus, a comparison with the linear theory is justified. Only the phase of the first harmonic component, ϕ_{p1} is shown. Unlike Case 1, the magnitude of higher harmonic components of Case 2 in the leading-edge region is not negligible (though small) because of the appearance of a local supersonic region there. The Euler computations of the fluctuating load magnitude and phase agree reasonably well with the experimental data. Their discrepancy is mainly associated with those in the magnitude of $(c_p)_{min}$ in Case 1 and the location of $(c_p)_{min}$ in both cases discussed in subsection A. Over the front portion of the airfoil the time-varying fluctuating load is nearly in phase with the airfoil pitching oscillation, and changes continuously to lag behind the oscillation towards the trailing edge. In Case 2, the experimental data show a larger phase lag than the Euler results towards the trailing edge. This is caused by the upper-surface boundary-layer thickening especially near the trailing edge observed in the experiments as reported by Ref. 16. The linear theory gives the qualitative behavior. The increase of the fluctuating load magnitude from Case 1 to Case 2 in both Case 1 and Case 2 are caused by the nonlinear contribution of mean angle of attack as discussed in Subsection B.

D. Force and Pitching Moment Variations

Figure 9 presents the computed instantaneous lift, pitching moment, and pressure thrust coefficients of the pitching airfoil versus ωt in a cycle compared with the experimental data[2] and incompressible linear theory. The instantaneous pitching moment and pressure thrust data for the cases considered in this paper are hard to be read out with enough accuracy from the plots in Ref. 2. A distinct discrepancy between the Euler computations and Experimental data appears in the lift and pitching-moment curves of Case 2. During the pitch-down motion, the experimental value of c_l becomes significantly less than the Euler value. The discrepancy in c_l is caused by the upper-surface boundary-layer thickening, especially near the trailing edge in Case 2.[16] The experimental c_m becomes larger than the Euler value when ωt increases from 0° to 270°. The reason for the discrepancy in c_m is unknown. Otherwise, the agreement between the Euler computations and experimental data are fair in considering the inaccuracy of the test data reading. The linear theory gives qualitative behavior.

The maximum lift coefficient $(c_l)_{max}$, the minimum pitching moment coefficient $(c_m)_{min}$ and minimum pressure thrust coefficient $(c_t)_{min}$ over a oscillation cycle were presented in the test report.[2] They are compared with the Euler computations and the linear theory in Table 2. Their agreements are fair.

Table 2 Comparison of the computed $(c_l)_{max}$, $(c_m)_{min}$, and $(c_t)_{min}$ of pitching NACA 0012 airfoil followed by α at which it occurs with the experimental data[2] and linear theory.

case	Methods	$(c_l)_{max}$	$(c_m)_{min}$	$(c_t)_{min}$
1	Euler	1.04,9.90°	-0.0283,4.93°	-0.0386,9.08°
1	Exp	1.13,10.0°	-0.04,4.7°	$-0.05, 9.1°$
1	Linear	0.964,9.97°	-0.0275,5.0°	$-0.0296, 8.82°$
2	Euler	1.40,12.9°	-0.0315,7.49°	$-0.055, 12.1°$
2	Exp	1.45,12.9°	-0.025,7.0°	-0.050,11°
2	Linear	1.29,13.0°	-0.0275,7.48°	-0.041,11.5°

E. Effects of Mean angle of Attack

Mean angle of attack has a nonlinear effect on fluctuating pressure and load as seen in Subsections B and C. Figure 10 presents computed instantaneous pressure thrust coefficient c_t (left), and input power coefficient c_{ip} of the airfoil versus the instantaneous pitching angle of attack $(\alpha - \alpha_0)$ for $\alpha_0 = 0$, 5° and 8° and $\alpha_1 = 5°$.

In the case of $\alpha_0 = 0$, consider one position of the oscillating airfoil during pitch-up and another position during pitch-down, and their locations are symmetric with respect to the neutral position. The flows about the two symmetric positions during pitch-up and pitch-down are mirror-symmetric with respect to the neutral position. The instantaneous thrusts are, therefore, equal for the two symmetric positions during pitch-up and pitch-down. (The instantaneous lifts are equal in magnitude but opposite in sign for the symmetric positions during pitch-up and pitch-down.) The curves c_t for pitch-up and pitch-down are symmetric with

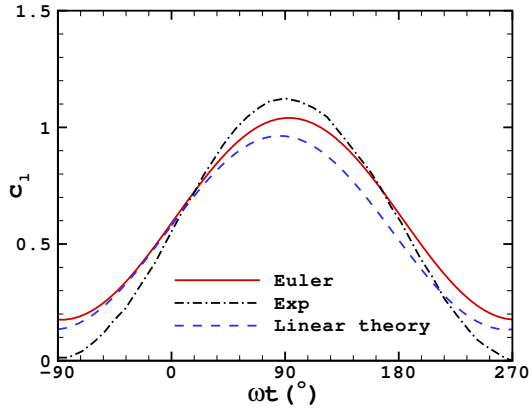

(a) Case 1

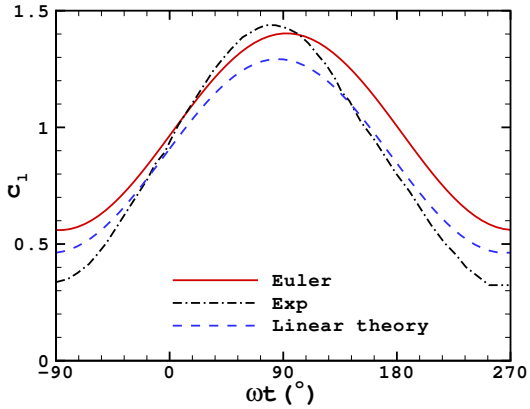

(b) Case 2

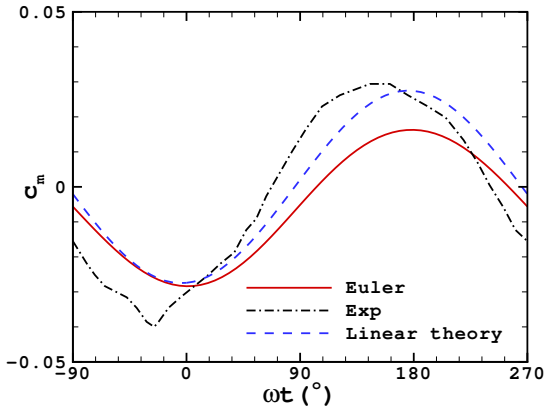

(c) Case 1

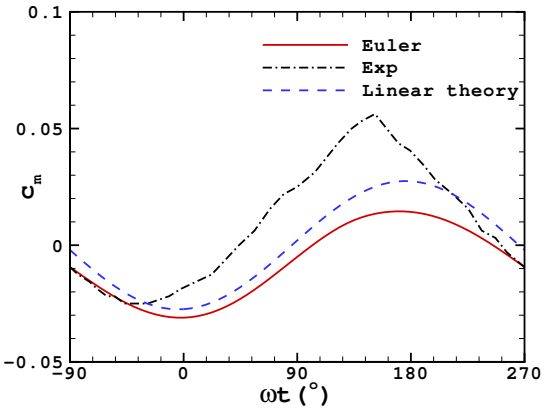

(d) Case 2

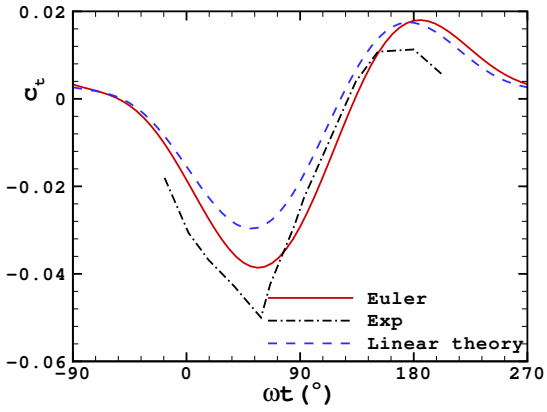

(e) Case 1

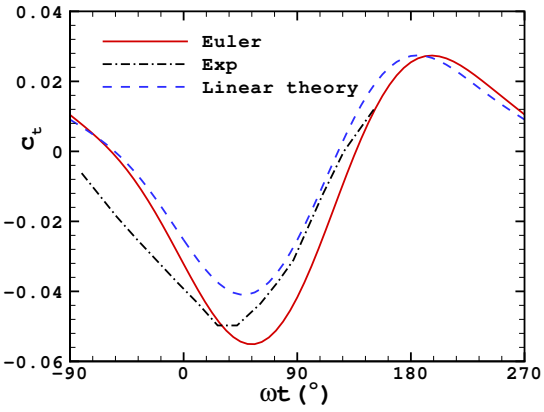

(f) Case 2

Figure 9. Instantaneous lift, pitching moment, and pressure thrust coefficients versus ωt.

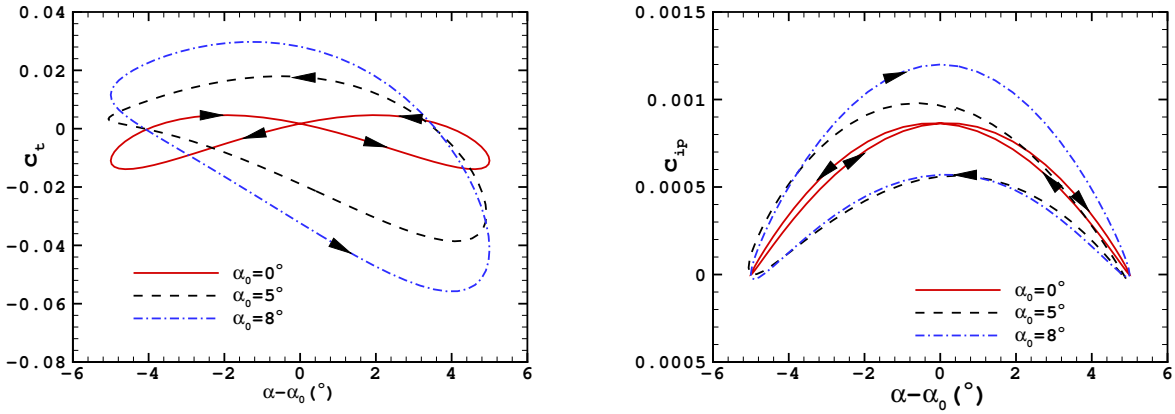

(a) Pressure thrust coefficient

(b) Input power coefficient

Figure 10. Instantaneous pressure thrust coefficient , and instantaneous input power coefficient.

respect to the ordinate as shown in Fig. 10. The curve c_t over a pitching-oscillation cycle forms two loops mirror-symmetric to the ordinate and has a double frequency. A non-zero mean angle of attack changes the scenario entirely. The curve c_t over a cycle forms one loop and has the same frequency as the airfoil oscillation. The instantaneous input power has similar behavior as shown in the right figure. The pressure thrust during pitch-down is greater than that during pitch-up, and the input power during pitch-down is smaller than that during pitch-up.

V. Conclusions

Two no-stall cases from a standard data base of wind tunnel tests for sinusoidal pitching NACA 0012 airfoil at free-stream Mach number of 0.3 are computed by the time-accurate compressible Euler method. One case is of subcritical flow and the other is supercritical. The wind-tunnel walls are not considered in the present computations. The unsteady pressure distributions and the instantaneous and time-averaged aerodynamic forces and moment, typical flow fields, and effects of mean angle of attack are studied extensively in comparison with the tests and the incompressible linear theory.

The Euler solutions agree reasonably well with the available experimental data. For the supercritical case, the experimental maximum Mach number of 1.232 with no shock patterns, and the constant minimum pressure coefficient of -9.1 at the dynamic stall boundary are closely reproduced. For the subcritical case, the Euler method under-predicts the suction peak on the leading edge upper surface, which may be due to the observed small laminar-boundary-layer separation bubble near the upper surface leading edge. An over-prediction of lift during pitch-down in the supercritical case may be caused by the observed upper-surface boundary-layer thickening, especially near the trailing edge.

The mean angle of attack has nonlinear effects on the fluctuating pressure and the instantaneous thrust and input power distributions over a motion cycle. The fluctuating load increases with mean angle of attack. The frequency of instantaneous thrust and input power change from double to single of the motion frequency due to nonzero mean angle of attack.

The classical incompressible linear theory gives the right qualitative behavior, but not accurate due to the flow compressibility and finite disturbance.

References

[1]McCroskey, W. J., McAlister, K. W., Carr, L. W., Pucci, S. L., Lambert, O., and Indergrand, R., "Dynamic stall on advanced airfoil sections," *Journal of the American Helicopter Society*, Vol. 26, 1981, pp. 40–50.

[2]McAlister, K. W., Pucci, S. L., McCroskey, W. J., and Carr, L. W., "An experimental study of dynamic stall on advanced airfoil sections, Volume 2, Pressure and force data," NASA TM 84245, Sept. 1982.

[3]Fung, K.-Y. and Carr, L. W., "Effects of compressibilty on dynamic stall," *AIAA Journal*, Vol. 29, 1991, pp. 306–308.

[4]Garrick, I. E., "Propulsion of a flapping and oscillating airfoil," NACA REPORT No. 567, May 1936.

[5]Theodorsen, T., "General theory of aerodynamic instability and the mechanism of flutter," NACA REPORT No. 496, May 1934.

[6]Biot, M. A., "Some simplified methods in airfoil theory," *J. Aeronautical Sciences*, Vol. 9, 1945, pp. 186–190.

[7]Fung, Y. C., *An Introduction to the Theory of Aeroelasticity*, Dover, New York, 1993.

[8]McCroskey, W. J., "Unsteady airfoils," *Ann. Rev. Fluid Mech.*, Vol. 14, 1982, pp. 285–311.

[9]Neef, M. F. and Hummel, D., "Euler solutions for a finite-span flapping wing," Tech. rep., Conference on fixed, flapping and rotary wing vehicles at very low Reynolds numbers, Univesity of Norte Dame, IN. June 2000.

[10]Yang, S., Luo, S., Liu, F., and Tsai, H.-M., "Computation of the flows over flapping airfoil by the Euler equations," AIAA Paper 2005-1404, Jan. 2005.

[11]Tuncer, I.H. Walz, R. and Platzer, M., "A computational study on the dynamic stall of a flapping airfoi," AIAA Paper 1998-2519, June 1998.

[12]Isogai, K., Shinmoto, Y., and Watanabe, Y., "Effects of dynamic stall on propulsive efficiency and thrust of flapping airfoil," *AIAA Journal*, Vol. 37, 1999, pp. 1145–1151.

[13]Young, J. and Lai, J. C. S., "Oscillation frequency and amplitude effects on the wake of a plunging airofil," *AIAA Journal*, Vol. 42, 2004, pp. 2042–2052.

[14]Ho, C.-M. and Chen, S.-H., "Unsteady wake of a plunging airfoil," *AIAA Journal*, Vol. 19, 1981, pp. 1492–1494.

[15]Yang, S., Luo, S., Liu, F., and Tsai, H.-M., "Supercritical Flow over Unstalled Plunging Airfoil Computed by Euler Method," AIAA Paper 2006-0293, Jan. 2006.

[16]McCroskey, W. J. and Pucci, S. L., "Viscous-inviscid interaction on oscillating airfoils in subsonic flow," *AIAA Journal*, Vol. 20, 1982, pp. 167–174.

[17]Cai, J., Tsai, H.-M., Luo, S., and Liu, F., "Stability of vortex pairs over slender conical bodies– theory and numerical computations," AIAA Paper 2004-1072, Jan. 2004.

[18]Liu, F. and Jameson, A., "Multigrid Navier-Stokes calculations for three-dimensional cascades," *AIAA Journal*, Vol. 31, No. 10, October 1993, pp. 1785–1791.

[19]Liu, F. and Zheng, X., "A strongly-coupled time-marching method for solving the Navier-Stokes and k-ω turbulence model equations with multigrid," *J. of Computational Physics*, Vol. 128, 1996, pp. 289–300.

[20]Liu, F. and Ji, S., "Unsteady flow calculations with a multigrid Navier-Stokes method," *AIAA Journal*, Vol. 34, No. 10, Oct. 1996, pp. 2047–2053.

[21]Sadeghi, M., Yang, S., and Liu, F., "Parallel computation of wing flutter with a coupled Navier-Stokes/CSD method," AIAA Paper 2003-1347, Jan. 2003.

[22]Yang, S., Luo, S., Liu, F., and Tsai, H.-M., "Trailing-edge flow about unstalled plunging airfoil computed by Euler method," Aiaa paper, submitted to 24th AIAA Applied Aerodynamics Conference, San Francisco, CA, 5-8 June, 2006.

[23]Jones, K. D., Dohring, C. M., and Platzer, M. F., "Experimental and computational investigation of the Knoller-Betz effect," *AIAA Journal*, Vol. 36, 1998, pp. 1240–1246.

[24]Lewin, G. C. and Haj-Hariri, H., "Modelling thrust generation of a two-dimensional heaving airfoil in a viscous flow," *J. Fluid Mech.*, Vol. 492, 2003, pp. 339–362.